Environ. Sci. Technol. **2007**, *41,* 1689−1695

Study of an Axial Flow Cyclone to Remove Nanoparticles in Vacuum

CHUEN-JINN TSAI,*,† SHENG-CHIEH CHEN,† RAFAL PRZEKOP,†,‡ AND ARKADIUSZ MOSKAL‡

Institute of Environmental Engineering, National Chiao Tung University, no.75 Poai Street, Hsin Chu, 300, Taiwan, and Department of Chemical and Process Engineering, Warsaw University of Technology, Warynskiego 1, 00-645 Warsaw, Poland

An axial flow cyclone for removing nanoparticles was tested for collection efficiency. Data were validated numerically in vacuum conditions of several Torrs, with flow rates of 0.35−0.57 slpm. The experimental cutoff aerodynamic diameter of the cyclone ranged from 21.7 to 49.8 nm. A 3-D numerical simulation was conducted first to calculate detailed flow and pressure fields, then a Brownian Dynamics simulation was done to determine the collection efficiency of nanoparticles. Both centrifugal force and Brownian diffusion were taken into account. The simulated results for both pressure drop and cutoff aerodynamic diameter are in good agreement with the experimental data. In comparison, previous theories using simplified tangential flow field assumption are not able to predict collection efficiencies accurately. The numerical model developed in this study can facilitate cyclone design to classify valuable nanopowders below a certain diameter, or to remove toxic nanoparticles from the vacuum exhaust of process chambers commonly used in high-tech industries.

Introduction

Cyclone separators are well-known dust separators or particle sampling devices whose operation is based on particle centrifugal force created by the vortex flow in the cyclone. The two most commonly used cyclones are tangential and axial flow cyclones, which are classified according to the entry direction of the gas stream. Research studies on tangential flow cyclones have extensively examined cutoff diameter (*1*−*3*) and collection efficiency (*1*−*2*, *4*−*7*). After reviewing theories and comparing them with published experimental data (*3*, *7*, *9*−*11*), Kao and Tsai (*8*) concluded that none of the existing theories predicts the cutoff diameter and collection efficiency accurately within the whole range of the flow Reynolds number, which is based on the dimension of the cyclone radius minus the exit-tube radius.

In contrast, only a few researchers have studied the axial flow cyclone, such as the experimental work of Liu and Rubow (*12*), Weiss et al. (*13*) and Vaughan (*14*), and the theoretical work of Maynard (*15*). These researchers studied the axial flow cyclone operating in ambient conditions. Liu and Rubow (*12*) developed an axial flow cascade cyclone at a design flow rate of 30 slpm for sampling particles of high concentration, with cutoff aerodynamic diameters of five stages at 12.2, 7.9, 3.6, 2.05, and 1.05 μm, respectively. Maynard (*15*) was the first to theoretically study particle penetration of the axial flow cyclone operating at ambient pressure. He proposed an implicit equation for particle penetration based on the assumption that particle collection mainly occurs in the vane and body sections. The equation predicts the cutoff aerodynamic very well at ambient pressures for the geometry and flow rates studied.

Tsai et al. (*16*) designed and tested an axial flow cyclone to remove nanoparticles operating in vacuum conditions of several torrs. The inner radius of the cyclone (r_{max}) and the radius of the vane spindle (r_{min}) were 15 and 10 mm, respectively. The cutoff aerodynamic diameter of the cyclone was found to be 43 nm, when the cyclone inlet pressure (P_{in}) is 6 torrs at a flow rate of 0.455 slpm. Tsai et al. (*16*) also proposed a theoretical equation based on the volumetric flow rate, the geometry of the cyclone, the properties of the carrying gas, and the pressure in the cyclone to predict particle collection efficiency. The tangential flow profile in the vane section was assumed to be plug flow. The cutoff aerodynamic diameter D_{pa50} for the cyclone with N vanes was derived to be

$$D_{pa50} = 0.106\left(\frac{P_{cyc}}{P_{760}}\right)^2 \frac{\mu(r_{max}^2 - r_{min}^2)(B - Nw)}{\rho_{po} n\zeta Q_0 r_{min}^2 N^2 \lambda_0} \quad (1)$$

Where μ is the fluid dynamic viscosity [Ns/m^2], B is pitch of vanes [m], w is the vane thickness [m], ρ_{po} is unit density (1000 kg/m^3), λ_0 is the mean free path of air molecules at standard conditions [m], Q_0 is the standard volumetric flow rate [m^3/s], P_{cyc} is the average of the pressure at the cyclone inlet (P_{in}) and outlet (P_{out}) [Torr], P_{760} is 760 Torr and $n\zeta$ is the total number of turns of a particle in the cyclone, assuming that the vortex makes n turns in the vane and additional $n(\zeta$-1) turns downstream from the vane. ζ was chosen to be 1.5 to give the best fit to the experimental data. The equation agrees well with the experimental data (*12*−*14*) in ambient conditions. However, at low-pressure conditions, the equation predicts much smaller cutoff aerodynamic diameters than the experimental data. The flow Reynolds number was shown to be an important factor that must be included in a theoretical equation to predict D_{pa50} accurately. An empirical equation based on the flow Reynolds number was therefore proposed by Tsai et al. (*16*) to predict the cutoff aerodynamic diameter.

Hsu et al. (*17*) studied the particle collection efficiency theoretically and experimentally using the axial flow cyclone designed by Tsai et al. (*16*). The authors derived an equation to predict the particle collection efficiency in which both centrifugal and diffusional forces were taken into account. Similar to Tsai et al. (*16*), plug flow assumption was made for the tangential flow in the vane section. The collection efficiency derived by Hsu et al. (*17*) is

$$\eta = 1 - \exp\left[-\left(\frac{D_{pa50,diff}}{D_{pa}} + \frac{D_{pa}^2}{D_{pa50}^2}\right)\right] \quad (2)$$

where the centrifugal cutoff aerodynamic diameter D_{pa50} is

$$D_{pa50} = \sqrt{\frac{9\mu(r_{max}^2 - r_{min}^2)^2(B - Nw)^2 \ln 2}{8\pi n\zeta Q_0 r_{min}^2 N^2 BC}} \quad (3)$$

* Corresponding author phone: +886-3-5731880; fax: +886-3-5731880; e-mail: cjtsai@mail.nctu.edu.tw.
† National Chiao Tung University.
‡ Warsaw University of Technology.

10.1021/es060518o CCC: $37.00
Published on Web 01/23/2007

and the diffusive cutoff aerodynamic diameter $D_{pa50,diff}$ is

$$D_{pa50,diff} = \frac{4n\zeta kTC}{3Q_0\mu \ln 2} \quad (4)$$

where C is the slip correction factor, k is boltzmann's constant, and T is the absolute temperature [K]. For a flow rate of 0.455 slpm and cyclone pressure of several Torrs, eq 2 predicts centrifugal force is the predominant mechanism for particle removal when particles are larger than 40 nm in aerodynamic diameter. For particles smaller than 40 nm in diameter, diffusional deposition is the main mechanism. Below 40 nm, the collection efficiency of nanoparticles increases with decreasing particle size. Experimental data presented by Hsu et. al (*17*) show similar trends, but substantial disagreement exists between theoretical results and experimental data.

The cyclone flow field is three-dimensional and cannot be expressed by simple equations. The simple plug flow assumption used by Tsai et al. (*16*) and Hsu et al. (*17*) could lead to inaccurate predictions of particle collection efficiency or of cutoff diameter. In addition, it is not certain whether the vortex flow after the vane section is still strong enough for particle removal after the vane. Accurate flow field and pressure distribution are the key factors influencing prediction of particle collection efficiency and cutoff diameter. Several researchers have numerically studied the flow fields of tangential flow cyclones and examined the influence of different geometries and operating conditions on their collection efficiencies (*18*−*23*). Recently, Gimbun et al. (*24*) used the CFD approach for modeling the tangential flow cyclone. Results obtained by the authors match very well with the experimental data obtained by Xiang et al. (*25*).

Given this context, this study's main objective was to obtain the flow field and pressure distribution in the axial cyclone of Tsai et al. (*16*) accurately by 3-D numerical simulation first, then to calculate particle collection efficiency. Finally, efficiency was validated by the experimental data obtained in this study and by those obtained by Hsu et al. (*17*). In addition to the centrifugal force, Brownian diffusion was also taken into account to predict the collection efficiency in the diffusion-controlled deposition regime.

Experimental Method

The experimental system is shown in Figure 1. Monodisperse OA (ρ_p = 894 kg/m^3) particles between 20 and 100 nm in diameter were generated by the atomization and electrostatic classification technique. Polydisperse particles were first generated by atomizing (Atomizer, TSI model 3076) 0.05 or 0.1% (v/v) OA solution. Then the aerosol flow was dried with a silica gel drier. The dried aerosol stream was passed through a furnace (Lindberg/Blue model CC58114C-1) at a fixed temperature at 650 K. The stream was then mixed with dry compressed air to produce sufficiently small particles (<100 nm). Monodisperse, single-charged particles were generated by classifying polydisperse particles using a nano-DMA (TSI model 3085).

The TSI Scanning Mobility Particle Sizer (SMPS) that includes a TSI model 3022 Condensation Particle Counter and a TSI model 3071 Electrostatic Classifier was used to monitor the concentrations of particles in the cyclone's inlet. The concentrations were used to correct for the multiple charge effect on the collection efficiency, which is typically less than 0−5%. For the detailed correction procedure, please refer to Tsai et al. (*16*).

An aerosol electrometer (TSI model 3068) was used to measure the electric current of the upstream and downstream aerosol concentrations in the cyclone. A critical orifice (O'Keefe Controls Co., E-8, 0.351 slpm or E-9, 0.455 slpm or E-10, 0.566 slpm) was installed at the cyclone inlet to achieve the desired flow rate and vacuum condition, which was

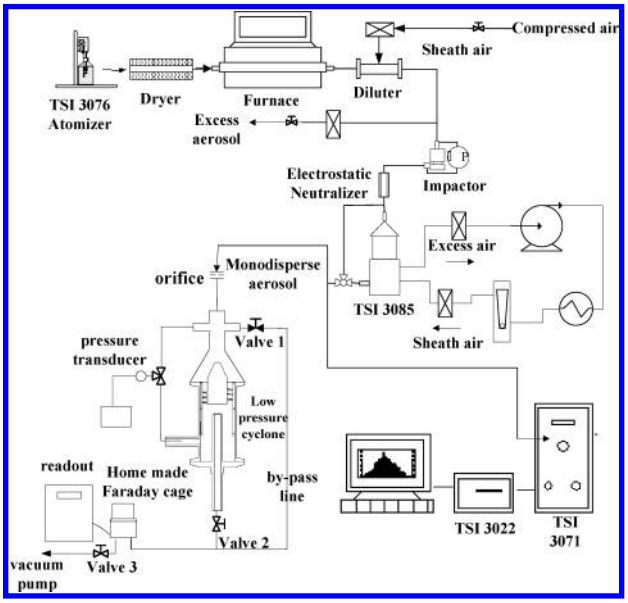

FIGURE 1. Experimental setup of the present study.

generated by a powerful vacuum pump (DUO 65, Pfeiffer, Germany, nominal pumping speed: 70 m^3/hr). The inlet pressures at the cyclone inlet were 4.3, 6.0, 5.4, 6.8, and 7.0 Torr.

In this study, particle concentration after the bypass line was found to be within 5% difference as compared to the concentration after the cyclone without the vane. Therefore, a bypass line was used to determine particle concentration at the cyclone inlet which could be controlled by an on−off valve (Valve 1) as shown in Figure 1. When Valve 1 is open and Valve 2 is closed, the aerosol flow will pass through the bypass line so that the inlet aerosol concentration can be measured. On the other hand, when Valve 1 is closed and Valve 2 is open, the aerosol flow will pass through the cyclone and the particle concentration at the cyclone outlet can be obtained. By adjusting the angle valve (Valve 3) downstream of the Faraday cage, the pressure at the cyclone inlet can be controlled.

The cyclone, spindle, and vane are shown in Figure 2(a) and 2(b). The radius of the spindle and the inner radius of the cyclone are 10 and 15 mm, respectively. Vane section width and height are 5 and 4 mm, respectively.

Numerical Method

Flow Field Simulation. In order to obtain accurate pressure distribution and flow velocity fields in the cyclone, 3-D numerical simulation was conducted for this study. The governing equations are Navier−Stokes and continuity equations. Since the maximum Kundsen number was 0.01 for this study, the flow was considered as a continuum. Steady-state laminar compressible flow was assumed, as well. The Navier−Stokes and the continuity equations were solved by using the Fluent CFD package based on the finite volume discretization method. Multiblock tetra cells were generated by the automatic mesh generation tool, Gambit. The total number of cells used was about 1 000 000 in the calculation domain, which includes the inlet and vane sections, the chamber after the vane, and the outlet tube as shown in Figure 2. The average cell length was around 0.5 mm and the smallest length of 0.1 mm was assigned near the surface of the vane. It was found that increasing the number of cells to 1 400 000 did not change the value of tangential velocity by more than 0.3−1.2%. Hence, a fixed cell number of 1 000 000 was used in this study.

The convergence criterion of the flow field calculation was set at 10^{-6} for the summation of the residuals. The total

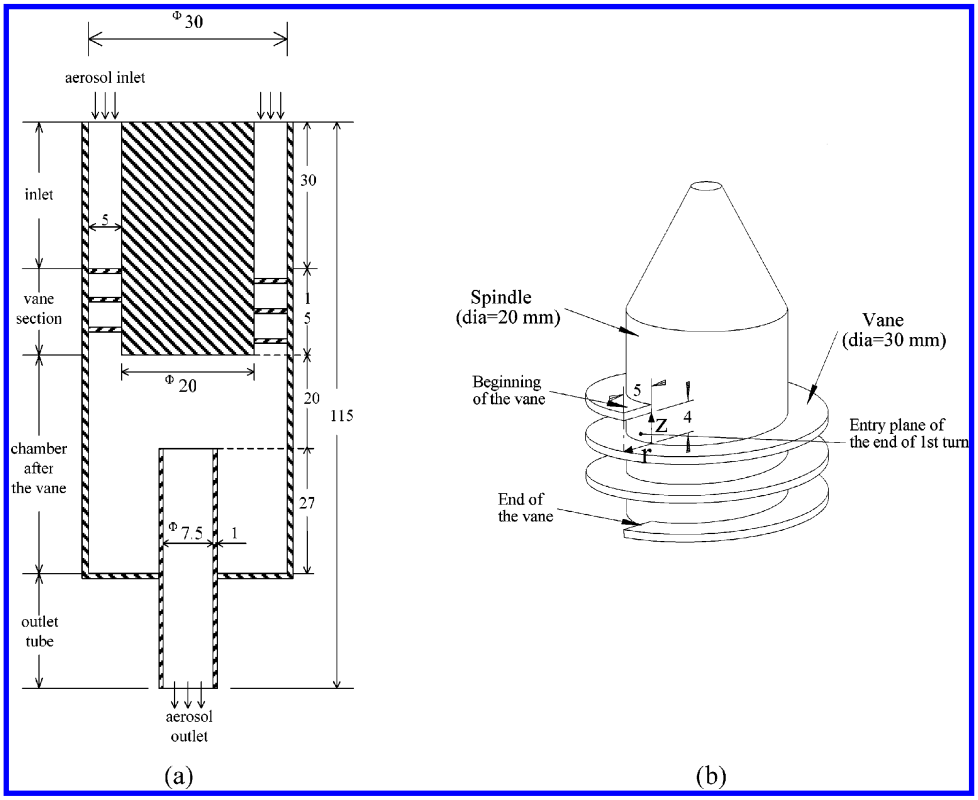

FIGURE 2. Schematic diagram of (a) cyclone (b) spindle and vane. (Unit = mm. The r−z coordinate and the dimension are also indicated.)

number of iterations was about 1000 and the time required to reach convergence was about 240 min. Non-slip conditioning was applied to the walls. A constant mass flow rate (0.351, 0.455, or 0.566 slpm) was set on the inlet boundary assuming uniform velocity profile. A fixed pressure, based on the experimental data. was assigned to the outlet boundary

Particle Collection Efficiency Simulation. For computing collection efficiency, the Lagrangian method was used for calculating particle trajectories. For each particle diameter, particle trajectories of 10 000 particles uniformly distributed in the inlet were calculated. When a particle touched the wall of the cyclone it was assumed to have been collected by the cyclone. Neither bounce-back nor resuspension of previously deposited particles were taken into account. The collection efficiency was calculated as the number of particles deposited in the cyclone divided by the number of particles entering the cyclone, or 10 000. This number was chosen to obtain reliable results in a reasonable computational time.

For small particles, the stochastic momentum exchange with bombarding gas molecules becomes significant. Brownian dynamics method was used to include the influence of diffusive motion on particle deposition. The equation of motion of the particle can be written as the following Langevin equation:

$$m\frac{d\boldsymbol{v}}{dt} = \boldsymbol{F}^{(\mathrm{D})} + \boldsymbol{F}^{(\mathrm{ext})} + \boldsymbol{F}^{(\mathrm{B})} \tag{5}$$

where m is the particle mass, $\boldsymbol{v}$ is the particle velocity, $\boldsymbol{F}^{(\mathrm{D})}$ is the drag force on the particle, $\boldsymbol{F}^{(\mathrm{ext})}$ denotes the external force, and $\boldsymbol{F}^{(\mathrm{B})}$ is the rapidly fluctuating, random force resulting from the particle bombardment by gas molecules. Thus $\boldsymbol{F}^{(\mathrm{B})}$ can be defined as

$$\boldsymbol{F}^{(\mathrm{B})} = m\boldsymbol{A}(t) \tag{6}$$

where $\boldsymbol{A}$(t) is the random acceleration of the particle. In this study, no external force was considered other than gravitational; however, gravity was found to be negligible compared to the drag force. The drag force is given by

$$\boldsymbol{F}^{(\mathrm{D})} = \frac{3\pi\mu d_{\mathrm{p}}}{C}(\boldsymbol{u} - \boldsymbol{v}) \tag{7}$$

where $\boldsymbol{u}$ is the local fluid velocity, d_{p} is the particle diameter, μ is fluid viscosity, and C is the Cunningham factor which can be expressed as

$$C = 1 + \left(\frac{2\lambda}{d_{\mathrm{p}}}\right)\left[1.257 + 0.400\exp\left(-0.55\frac{\lambda}{d_{\mathrm{p}}}\right)\right] \tag{8}$$

where λ denotes the mean free path of air molecules.

The Brownian Dynamics (BD) method was established by Chandrasekhar (*26*) for Stokesian particles in a stationary fluid ($\boldsymbol{u} = 0$) and force-free field ($\boldsymbol{F}^{(\mathrm{ext})} = 0$). The Chandrasekhar's first lemma was

$$\boldsymbol{R} = \int_0^t \psi(\xi)\boldsymbol{F}^{(\mathrm{B})}(\xi)/m d\xi \tag{9}$$

The function $\psi(\xi)$ was defined to be

$$\psi(\xi) = \tau\left(1 - \left[\exp\left(\frac{\xi - t}{\tau}\right)\right]\right) \tag{10}$$

where τ is the particle relaxation time

$$\tau = \frac{\rho_p d_p{}^2 \mathrm{C}}{18\mu} \tag{11}$$

ρ_{p} is the particle density. Then the probability distribution of $\boldsymbol{R}$ is given by

$$\vartheta(\boldsymbol{R}) = \frac{\exp[-|\boldsymbol{R}|^2/4q\int_0^t \psi^2(\xi)d\xi]}{[4\pi q\int_0^t \psi^2(\xi)d\xi]^{3/2}} \quad (12)$$

where q is defined as

$$q = \frac{kT}{\tau m} \quad (13)$$

From eq 12, expected values of particle displacement in the ith direction $<\Delta L_i>$ and its velocity change $<\Delta v_i>$ during time interval Δt can be found as

$$<\Delta L_i> = v_i\tau[1 - \exp(-\Delta t/\tau)] \quad (14)$$

$$<\Delta v_i> = v_i[1 - \exp(-\Delta t/\tau)] \quad (15)$$

The standard deviations of displacement σ_{Li} and particle velocity change σ_{vi} has been derived to be

$$\sigma_{vi} = \sqrt{(1 - \exp(-2\Delta t/\tau))k_B T/m} \quad (16)$$

$$\sigma_{Li} = \sqrt{(2\Delta t/\tau - 3 + 4\exp(-\Delta t/\tau) - \exp(-2\Delta t/\tau)k_B T/(m/\tau^2)} \quad (17)$$

In this study, extension of BD in the case of moving fluid with external forces derived by Podgórski (*27*) was used. Integration of the Langevin equation for a time interval small enough so that the host fluid velocity $\boldsymbol{u}$ and external forces $\boldsymbol{F}^{(ext)}$ may be assumed constant over $(t, t + \Delta t)$, gives the following bivariate normal density probability distribution function, $\vartheta_i(\Delta v_i, \Delta L_i)$,

$$\vartheta_i(\Delta v_i,\Delta L_i) = \frac{1}{2\pi\sigma_{vi}\sigma_{Li}\sqrt{1-\rho_c}}\exp\left\{-\frac{1}{2(1-\rho_c^2)}\left[\left(\frac{\Delta v_i - \langle\Delta v_i\rangle}{\sigma_v i}\right)^2 + -\frac{2\rho_c(\Delta v_i - \langle\Delta v_i\rangle)(\Delta L_i - \langle\Delta L_i\rangle)}{\sigma_{vi}\sigma_{Li}} + \left(\frac{\Delta L_i - \langle\Delta L_i\rangle}{\sigma_{L_i}}\right)^2\right]\right\} \quad (18)$$

where ρ_c is the coefficient of correlation.

The distribution may be rearranged to a more convenient form as the product of two Gaussian distributions:

$$\vartheta_i(\Delta v_i,\Delta L_i) = \left\{\frac{1}{\sqrt{2\pi}\sigma_i}\exp\left[-\frac{1}{2}\left(\frac{\Delta v_i - <\Delta v_i>}{\sigma_{vi}}\right)^2\right]\right\}\left\{\frac{1}{\sqrt{2\pi(1-\rho_c^2)}\sigma_{Li}}\exp\left[-\frac{1}{2}\left(\frac{\Delta L_i - <\Delta L_i> - \rho_c\sigma_{Li}(\Delta v_i - <\Delta v_i>)/\sigma_{vi}}{\sigma_{Li}\sqrt{1-\rho_c^2}}\right)^2\right]\right\} \quad (19)$$

The expected values of particle velocity change $<\Delta v_i>$ and the linear displacement $<\Delta L_i>$ are then equal to

$$<\Delta v_i> = [u_i - v_i + F_i^{(ext)}/(m/\tau)][1 - \exp(-\Delta t/\tau)] \quad (20)$$

$$<\Delta L_i> = [u_i + F_i^{(ext)}/(m/\tau)]\Delta t - [1 - \exp(-\Delta t/\tau)][u_i - v_i + F_i^{(ext)}/(m/\tau)]\tau \quad (21)$$

while standard deviations, σ_{vi}, σ_{Li}, are calculated by eq 16 and 17, respectively. The coefficient of correlation, ρ_c, is defined as

$$\rho_c = (1 - \exp(-\Delta t/\tau))^2[(1 - \exp(-2\Delta t/\tau))(2\Delta t/\tau - 3 + 4\exp(-\Delta t/\tau) - \exp(-2\Delta t/\tau))]^{-1/2} \quad (22)$$

We can therefore formulate the following generalized algorithm for the Brownian dynamics simulation. For a given initial particle position and its initial velocity components, v_i, at a moment t, we calculated the fluid velocity, u_i, and the external forces, $\boldsymbol{F}_i^{(ext)}$. Then, we calculated expected values $<\Delta v_i>$, $<\Delta L_i>$ from eqs 20−21, the standard deviations σ_{vi}, σ_{Li}, from eqs 16−17, and the correlation coefficient, ρ_c from eq 22. Next, we generated two independent random numbers, G_{Li}, G_{vi}, having Gaussian distribution with zero mean and unit variance. Finally, we calculated the change of the particle velocity, Δv_i, and the particle linear displacement, ΔL_i, during the time-step Δt from the expression accounting for deterministic and stochastic motion as

$$\Delta v_i = <\Delta v_i> + G_{vi}\sigma_{vi} \quad (23)$$

$$\Delta L_i = <\Delta L_i> + \rho_c G_{vi}\sigma_{Li} + (1 - \rho_c^2)G_{Li}\sigma_{Li} \quad (24)$$

All the above steps are repeated for each coordinate, $i = 1, 2, 3$. Having determined the increments Δv_i and ΔL_i according to eqs 20−21, the new particle velocity $v_i(t + \Delta t) = v_i + \Delta v_i$ and the new particle position is calculated. After completing this one-time simulation step, the next step was performed in the same way. The time step was calculated as the minimum side-length of each cell divided by the flow velocity at the cell center. Decreasing the time step was shown not to affect the simulated collection efficiency. The computation of the particle trajectory stops when the particle touches the wall or exits the computation domain. After calculating the trajectories of all 10 000 particles at the inlet, the collection efficiency of the particle could be determined.

Results and Discussion

Tangential Flow and Pressure Distributions in the Cyclone. Figure 3 shows the tangential velocity distributions in the vertical cross sections at $r = 2.5$ mm along the vane section of the cyclone, when $P_{in} = 5.4$ Torr, and $Q = 0.455$ slpm. Please refer to Figure 2(b) for the r−z coordinate system. The tangential velocity is seen to develop very fast in the vane section. At the end of the first rotation of the vane, the tangential velocity is still small and similar to plug flow. However, after 1.5 turns it develops into a parabolic-flow-like distribution and the peak tangential velocity increases along the vane section. In the horizontal cross sections at $z = 2.0$ mm, tangential velocity distributions are similar to

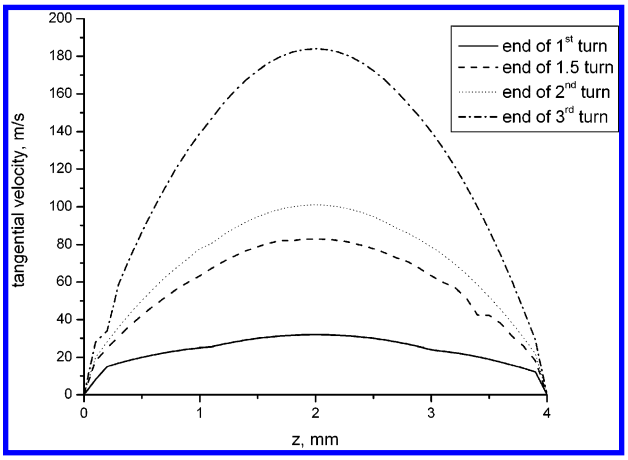

FIGURE 3. Velocity distribution in the cyclone, $Q = 0.455$ slpm, $P_{in} = 5.4$ Torr.

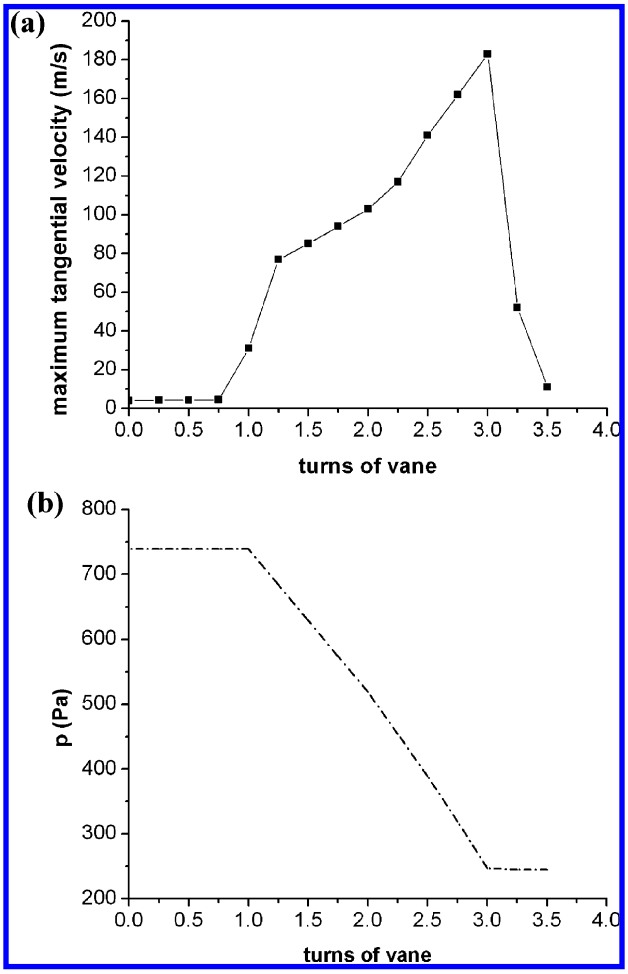

FIGURE 4. (a) Maximum tangential velocity and (b) pressure distribution in the vane section, numerical results, $Q = 0.455$ slpm, $P_{in} = 5.4$ Torr.

those shown in Figure 3. For other inlet pressure and flow-rate conditions, tangential velocity distributions are also similar.

Simulated results for the pressure distribution and maximum tangential velocity in the vane section for $P_{in} = 5.4$ Torr, and $Q = 0.455$ slpm are shown in Figures 4(a) and 4(b), respectively. It can be seen that the peak tangential velocity remains small in the first 3/4 turn of the vane section, after which it increases sharply and then exponentially until the end of three turns when the tangential velocity peaks at 184 m/s. After the flow exits the vane, the peak tangential velocity drops sharply until it becomes nearly 0 at 3.5 turns.

The variation of peak tangential flow velocity along the vane section corresponds very well with the variation of the pressure distribution shown in Figure 4(b). The pressure remains at about 740 Pa (or 5.5 Torr, which is within 2% of the experimental data) in the first turn and then drops monotonically in the second and third turns. The flow is accelerated in the tangential direction as the pressure is decreased in the vane. This is to be expected in accordance with ideal gas law in which the tangential flow-velocity increase is due to the air-density decrease as pressure is decreased. Finally, the pressure remains nearly constant at 260 Pa (or 1.95 Torr) after the end of the third turn. That is, the pressure drop occurs almost entirely in the second and third turns. This implies that the flow does not make three full turns as the vane does. Rather, it makes slightly more than two turns only. This is one of the main reasons for the large differences between the experimental cutoff aerodynamic diameters and the theoretical values in Tsai et al. (*16*) and Hsu et al. (*17*) in which the tangential flow was assumed to make three full turns in the vane section and the tangential velocity was assumed to be plug flow. The paraboloid flow profile in the vane section will result in a smaller collection efficiency and a larger cutoff diameter than the plug flow profile. Because of small flow rate and small flow Reynolds number for the cyclone, the tangential flow dissipates after the vane section, and there will be no further particle collection due to the centrifugal force after the vane section. A fitting parameter ζ of 1.5 used in the Tsai et al. (*16*) and Hsu et al. (*17*) models, assuming that an additional 1.5 turns of the vortex flow occurred after the vane section, would result in a higher collection efficiency and lower cutoff diameter than the experimental data suggests.

TABLE 1. Pressure Drop and Cutoff Aerodynamic Diameter for Different Operating Conditions

Q(slpm)	0.351	0.455	0.566	0.566	0.455
P_{in}(Torr)	4.31	5.43	6.77	7.00	6.00
ΔP_{num}(Torr)	2.93	3.65	4.79	4.16	2.82
ΔP_{exp}(Torr)	2.85	3.58	4.58	4.03	2.73
Δp_{50num}(nm)	22.39	23.40	26.65	36.98	50.03
Δp_{50num}(nm)[a]	22.54	23.59	27.27	37.35	50.92
Δp_{50exp}(nm)	21.69	23.14	25.58	36.65	49.75

[a] Brownian diffusion is neglected.

For different operating conditions, Table 1 summarizes a comparison of numerical pressure drop and cutoff aerodynamic diameter with the experimental data. The comparison shows that the numerical pressure drop is in excellent agreement (within 3.3% of error) with the experimental data. The agreement between the experimental data and the numerical results is also observed in the cutoff aerodynamic diameter, which is from about 20 to 50 nm for the operating conditions listed in Table 1. The maximum deviation is 6.2% for $Q = 0.566$ slpm and $P_{in} = 6.77$ Torr. For other conditions, the deviation is less than 4%.

Particle Collection Efficiency. The current experimental particle collection efficiencies and numerical results of the Brownian Dynamics simulation are shown in Figure 5 for the operating conditions of $P_{in} = 6.0$ and 7.0 Torr, and in Figure 6 for $P_{in} = 4.31$, 5.43, and 6.77 Torr, respectively. In Figure 5(a) and (b), the collection efficiency curves with and without considering Brownian diffusion are compared for $P_{in} = 6$ and 7.0 Torr, respectively. When Brownian diffusion is considered, the present numerical results agree with the experimental collection efficiencies very well for both inlet pressures in the whole range of diameters studied. Without considering Brownian diffusion, the numerical collection efficiencies still match very well with the experimental data for particles greater than the cutoff diameter; however, they are lower than the experimental data when particles are smaller than the cutoff diameter. The largest difference of 12.5% occurs at the smallest particle diameter of 27 nm (Figure 5(a)). The increase in the diffusional deposition was found to occur mainly in the chamber after the vane section when the gas expands and slows down, and there was no increase of the collection efficiency due to short residence time of particles in the vane section. For particles greater than the cutoff size, the centrifugal force dominates and whether or not Brownian diffusion is considered does not make any difference in the collection efficiency curves. For the cutoff diameter, simulation considering Brownian diffusion results in smaller and more-accurate results than not considering Brownian diffusion when $P_{in} = 6$ and with 7 Torr. Table 1 also shows cutoff diameters of 36.98 and 50.03 nm (or 1.0 and 0.6% error) with consideration of Brownian diffusion, and 37.35 and 50.92 nm (or 1.9 and 2.3% error) without considering Brownian diffusion.

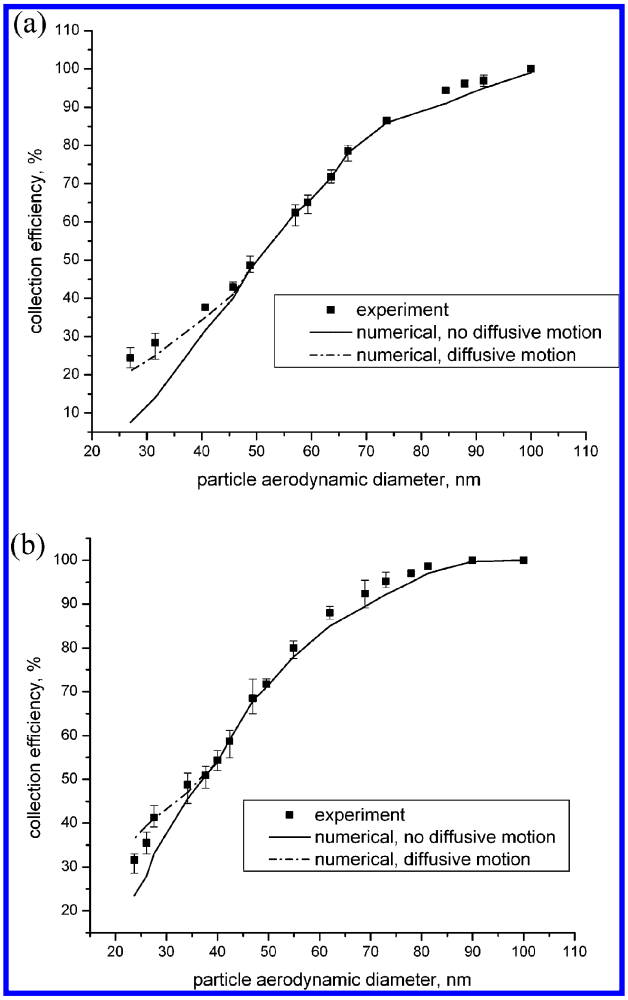

FIGURE 5. Comparison of numerical collection efficiencies and present experimental data, (a) P_{in} = 6.0 Torr; (b) P_{in} = 7.0 Torr.

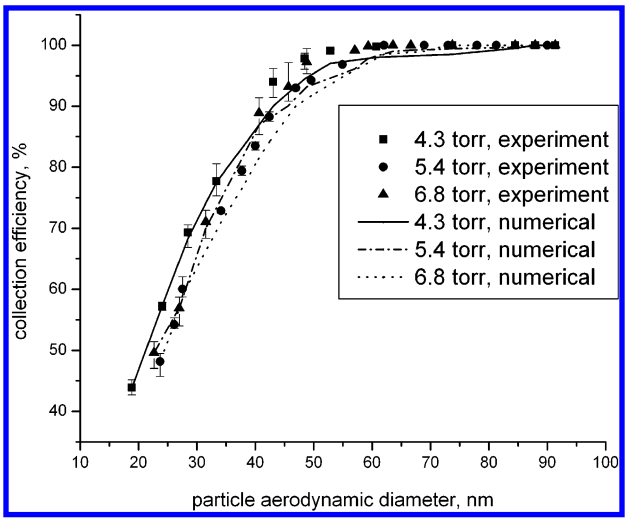

FIGURE 6. Comparison of numerical collection efficiencies and present experimental data, P_{in} = 4.3, 5.4, 6.8 Torr.

Figure 6 shows that all numerical results agree with the experimental collection efficiencies very well in the whole range of the cutoff aerodynamic diameter, when Brownian diffusion is considered. The error in the numerical cutoff aerodynamic is 3.2, 1.1, and 4.1%, for P_{in} = 4.31, 5.43, and 6.77 Torr, respectively. Neglecting Brownian diffusion in the simulation, particle collection efficiencies are similar to those in Figure 6, and the error in the cutoff aerodynamic diameter

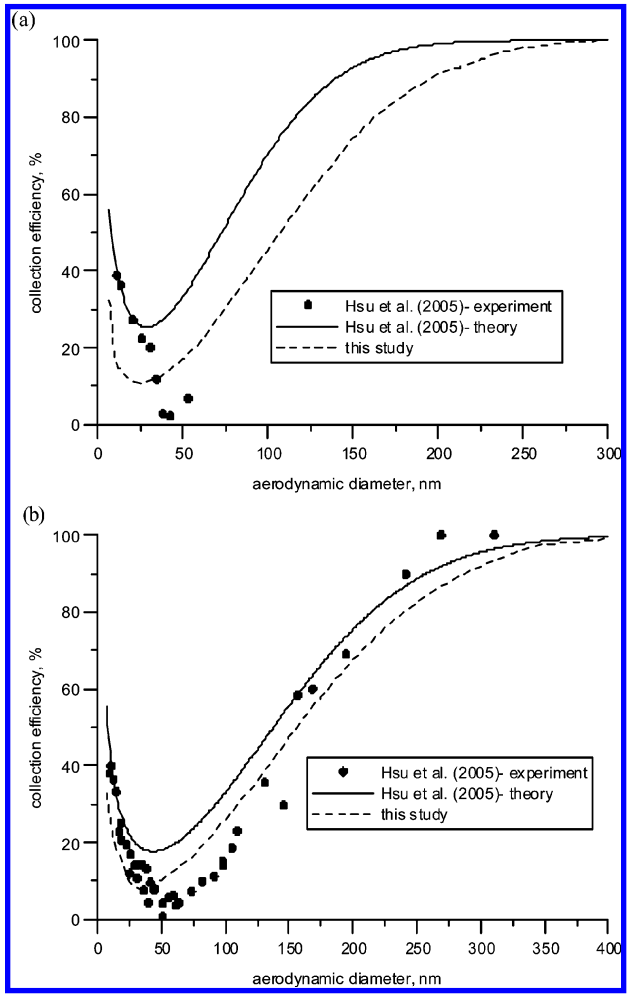

FIGURE 7. Comparison of the present numerical collection efficiencies with the experimental data and the theory by Hsu et al. (*17*); *Q* = 0.455 slpm (a) P_{out} = 4.8 Torr, (b) P_{out} = 6.5 Torr.

becomes slightly larger. The error is 3.8, 1.9, and 6.2% for P_{in} = 4.31, 5.43, and 6.77 Torr, respectively. These comparisons are also shown in Table 1. In Figure 6, few data points exist for particles below the cutoff aerodynamic diameter, since particle concentration becomes too low to obtain accurate efficiency data. If such data were available, Brownian diffusion would be expected to increase the collection efficiency for particles below the cutoff aerodynamic diameter similar to Figure 5.

Figure 7 (a) and (b) show the comparison of the numerical results of the present Brownian Dynamics calculations with experimental results obtained by Hsu et al. (17), for P_{out} = 6.5, and P_{out} = 4.8 Torr, respectively. The flow rate in both Figures is 0.455 slpm. It can be seen that the current Brownian Dynamics simulation predicts the collection efficiency reasonably well for both small and large particles in both cases. In comparison, the Hsu et al. (*17*) theoretical equation, eq 2, is less accurate than the simulation. The maximum error occurs near the minimum collection efficiency in eq 2, which overestimates the collection efficiency compared to current Brownian Dynamics calculations. This overestimation is suspected to be due to the simplified plug-flow assumption, and to assuming three rotations in the vane and the extra 1.5 rotations in the chamber. To investigate this matter further, we assumed two rotations of the flow in the vane section and no rotations in the chamber, or setting $n\xi = 2$, and used the Hsu et al. (17) model to recalculate the theoretical collection efficiency. It was found that substantial disagreement exists between the experimental data and the

theoretical results for particles greater than 100 nm. That is, not only the number of flow rotations must be accurate, but accurate flow and pressure profiles are also critical for obtaining accurate theoretical particle collection efficiency. The agreement of the calculated collection efficiencies of Hsu et al. (*17*) and the experimental data seen in Figure 7 based on $n\zeta = 4.5$ is just fortuitous.

In Figure 7, the collection efficiency due to diffusional deposition of small nanoparticles increases with decreasing diameter when the diameter is smaller than about 40−60 nm, which corresponds to the minimum collection efficiency. The current Brownian Dynamics simulation shows such diffusional deposition mainly occurs in the chamber after the vane section, not in the vane section. For example, the total numerical collection efficiency is 18.3% for 9.8 nm nanoparticles in Figure 7(a), in which 14.9% occurs in the chamber after the vane, and only 2.1% in the first turn of the vane and 1.3% in the vane between 1 and 1.5 turns.

In Figure 7(b), the total numerical collection efficiency is 18.5% for 11.34 nm nanoparticles, including 15.5, 1.8, and 1.2% in the chamber after the vane in the first turn, and the vane between 1 and 1.5 turns, respectively. The diffusional deposition is small in the cyclone's vane section as the flow residence time is usually small (on the order of 0.003 s) for the cyclone operating in vacuum conditions. In addition to the vane section, the theoretical prediction of particle deposition in the vane chamber is difficult due to the complexity of the flow field in it. The only way to calculate the collection efficiency of nanoparticles accurately is by numerical flow and particle simulation, such as the Brownian Dynamics simulation in this study.

Acknowledgments

We are thankful for the financial support of this project by Taiwan National Science Council (NSC 94-2211-E-009-001).

Literature Cited

(1) Lapple, C. E. Gravity and centrifugal separation. *Ind. Hyg. Q.* **1950**, *11*, 40−48.
(2) Barth, W. Design and layout of cyclone separator on the basis of new investigations. *Brennst.-Warme-Kraft* **1956**, *8*, 1−9.
(3) Iozia, D. L.; Leith, D. Effect of cyclone dimensions on gas flow pattern and collection efficiency. *Aerosol Sci. Technol.* **1989**, *10*, 491−500.
(4) Leith, D.; Licht, W. The collection efficiency of cyclone type particle collectors: a new theoretical approach. *AIChE Symp. Ser.* **1972**, *126*, 196−206.
(5) Dietz, P. W. Collection efficiency of cyclone separators. *AIChE J.* **1981**, *27*, 888−892.
(6) Li, E.; Wang, Y. A new collection theory of cyclone separators. *AIChE J.* **1989**, *35*, 666−669.
(7) Iozia, D. L.; Leith, D. The logistic function and cyclone fractional efficiency. *Aerosol Sci. Technol.* **1990**, *12*, 598−606.
(8) Kao, K. Y.; Tsai, C. J. On the theory of particle collection efficiency of cyclones. *Aerosol Air Qual. Res.* **2001**, *1*, 47−56.
(9) Zhu, Y.; Lee, K. W. Experimental study on small cyclones operating at high flowrates. *J. Aerosol. Sci.* **1999**, *30*, 1303−1315.
(10) Tsai, C. J.; Shiau, H. G.; Shih, T. S. Field study of the accuracy of two respirable sampling cyclones. *Aerosol Sci. Technol.* **1999**, *31*, 463−472.
(11) Dirgo, J.; Leith, D. Cyclone collection efficiency: Comparison of experimental results with theoretical predictions. *Aerosol Sci. Technol.* **1985**, *4*, 401−415.
(12) Liu, B. Y. H.; Rubow, K. L. A new axial flow cascade cyclone for size characterization of airborne particulate matter. In: Liu, B. Y. H.; Pui, D. Y., & Fissan, H. J. (Eds.), *Aerosols* (pp. 115−118). Amsterdam: Elsevier, 1984.
(13) Weiss, Z.; Martinec, P.; Vitek, J. *Vlastnosti Dulnibo Prachu A Zaklady Protiprasne Techniky;* SNTL: Prague, 1987.
(14) Vaughan, N. P. Construction and testing of an axial flow cyclone pre-separator. *J. Aerosol Sci.* **1988**, *19*, 295−305.
(15) Maynard, A. D. A simple mode of axial flow cyclone performance under laminar flow conditions. *J. Aerosol Sci.* **2000**, *31*, 156−167.
(16) Tsai, C. J.; Chen, D. R.; Chein, H. M.; Chen, S. C.; Roth, J. L.; Hsu, Y. D.; Li, W.; Biswas, P. Theoretical and experimental study of an axial flow cyclone for fine particle removal in vacuum conditions. *J. Aerosol Sci.* **2004**, *35*, 1105−1118.
(17) Hsu, Y. D.; Chein, H. M.; Chen, T. M.; Tsai, C. J. Axial flow cyclone for segregation and collection of ultrafine particle: Theoretical and experimental study. *Environ. Sci. Technol.* **2005**, *39*, 1299−1308.
(18) Boysan, F.; Ewan, B. C. R.; Swithenbank, J.; Ayers, W. H. Experimental and theoretical studies of cyclone separator aerodynamics. A*IChE Symp. Ser.* **1983**, *69*, 305−320.
(19) Hoekstra, A. J.; Derksen, J. J.; Van Den Akker, H. E. A. An experimental and numerical study of turbulent swirling flow in gas cyclones. *Chem. Eng. Sci.* **1999,** *54*, 2055−2065.
(20) Schmidt, S.; Thiele, F. Comparison of numerical methods applied to the flow over wall-mounted cubes. *Int. J. Heat Fluid Flow* **2002**, *23*, 330−339.
(21) Harwood, R.; Slack, M. CFD analysis of a cyclone. *QNET-CFD Network Newsletter* **2002**, *1*, 25−27.
(22) Schmidt, S.; Blackburn, H. M.; Rudman, M.; Sutalo, I. Simulation of turbulent flow in a cyclonic separator. In *3rd International conference on CFD in the Minerals and Process Industries CSIRO,* Melbourne, Australia, 10−12. December, 2003; Commonwealth Scientific and Industrial Research Organisation: Canberra, AU, 2003; pp 365−369.
(23) Xiang, R. B.; Lee, K. W. The flow pattern in cyclones with different cone dimensions and its effect on separation efficiency. In *Abstract, EAC 2004, Budapest, Hungary, Sep. 6−10*; pp. 289−290.
(24) Gimbun, J.; Chuah, T. G.; Choong, T. S. Y.; Fakhru'l-Razi, A. Prediction of the effects of cone tip diameter on the cyclone performance. *J. Aerosol Sc.* **2005,** *36*, 1056−1065.
(25) Xiang, R.; Park, S. H.; Lee, K. W. Effects of cone dimension on cyclone performance. *J. Aerosol Sc.* **2001,** *32*, 549−561.
(26) Chandrasekhar, S. Stochastic problems in physics and astronomy, *Rev. Mod. Phys.* **1943,** *15*, 1−89.
(27) Podgórski, A. *On the Transport, Deposition and Filtration of Aerosol Particles in Fibrous Filters: Selected Problems*; Oficyna Wydawnicza Politechniki Warszawskiej: Warsaw, 2002.

Received for review March 5, 2006. Revised manuscript received December 6, 2006. Accepted December 19, 2006.

ES060518O